Fermi National Accelerator Laboratory

FERMILAB-Conf-94/045-E

CDF

Jet Physics and QCD Tests at the Tevatron Collider

Robert Plunkett

Fermi National Accelerator Laboratory
P.O. Box 500, Batavia, Illinois 60510

February 1994

Presented at the *XIII International Conference on Physics in Collision*,
University of Heidelberg, Heidelberg, Germany, June 16-18, 1993

Disclaimer

CDF/PUB/JET/PUBLIC/2488
FERMILAB-CONF-94/045-E

JET PHYSICS AND QCD TESTS AT THE TEVATRON COLLIDER

Robert Plunkett
Fermi National Accelerator Laboratory
Batavia, Illinois 60510
USA

Abstract

Results are presented detailing the status of tests of perturbative QCD in hard parton-parton collisions generated by high energy collisions of protons and antiprotons at the Fermilab Collider. Recent data from the CDF and D0 experiments are compared to Next-to-Leading Order QCD calculations in hadronic jet production, prompt photon production,jet production in events with W bosons, and b-quark production.

XIII International Conference on Physics in Collision, University of Heidelberg, Heidelberg, Germany, June 16-18, 1993.

Introduction

Since the striking confirmation in 1982 of the existence of collimated jets of hadrons [1], it has been clear that high energy hadron colliders provide a rich source of tests of a variety of QCD predictions arising from both shower Monte Carlo calculations and perturbative calculations. Recently this development has accelerated as Next-to-Leading Order (NLO) calculations have become available for several processes, including inclusive jet production [2], the center-of-mass angular distribution of jets [3], and the production of jets associated with W intermediate vector bosons [4]. These calculations have removed significant theoretical uncertainties in the comparison of measurements of these quantities with QCD. For example, the expected normalization error due to renormalization scale variation on the transverse energy (E_t) distribution of inclusive jets has been reduced from (typically) 30% to 5% , thus presenting a considerable challenge to the experimenter. In addition, we now have available shower Monte Carlo calculations that include a variety of sophisticated color coherence effects, approximated either via an ordering scheme on the allowed radiation [5], or via a string model [6].

The Tevatron collider provides an excellent testing ground for many of these QCD predictions, both cross-sections and kinematical distributions. The high center-of-mass energy (1.8 TeV) and record beam luminosity (9×10^{30} cm^{-2} sec^{-1}) provide a high-statistics data sample covering a large fraction of the phase space available for hard scattering processes. The CDF experiment has previously published a number of QCD tests from earlier running periods. More recently the D0 experiment has come on line, and is rapidly producing interesting results.

This paper reviews data obtained at the Tevatron in the period 1992-93 at the CDF and D0 experiments. Results in the area of hadronic jet production are complemented by

measurements of vector boson + jet production for both photons and W bosons. In addition, I will discuss diphoton production at CDF, a D0 study of the dependence of the W + jet process on the strong coupling constant α_S, a preliminary observation of events with a depleted central region and jets ("rapidity gaps") by D0, and CDF techniques for extracting information on the parton distribution functions of the nucleon. Lastly, I will report on the measurement by CDF of the differential cross-section for the production of b-quarks, obtained using fully reconstructed B mesons.

QCD Jet Production

Hadronic jets are copiously produced at Tevatron energies, with a total cross-section on the order of 20 μb (depending on the threshold imposed). Since a jet has no rigid boundary, the rate produced will depend upon the algorithm chosen to define the jet; hence the importance of careful comparison with appropriate theoretical calculations. It has become the norm in hadron colliders to define jets using cone algorithms that take advantage of the natural kinematic variables of hadronic collisions, the "transverse energy" E_t and the pseudo-rapidity η. Both the CDF and D0 experiments use such jet algorithms. The cone radius is defined as $R = \sqrt{(\Delta\eta)^2 + (\Delta\phi)^2}$, where ϕ is the azimuthal angle w.r.t. the line defined by the colliding beams. Typical radii in use range from R=1.0 to R=0.4, depending on the needs of the specific analysis. CDF has examined the cone size dependences of the jet E_t and dijet mass spectra in refs [7,8]. The transverse energy is defined as $E\sin\theta$, where θ is the angle between the beamline and a line from the event vertex to the center of the jet cluster. Clusters are identified by an iterative process that begins by a search for seed calorimetry towers above a given E_t threshold (typically 1.0 GeV). Shared energy is either assigned to one or another of the clusters sharing it, or split between them, depending on the amount shared.

The most basic quantity in jet production is the E_t spectrum of inclusive jets. CDF and D0 have produced measurements of this distribution at various ranges of pseudo-rapidity. Figure 1 shows recent preliminary results from the two experiments, where the jet cross-section is evaluated in the central rapidity region. Also shown are NLO perturbative QCD calculations [2]. The level of agreement of the shape of the spectrum at high E_t can be used to set a limit on possible pointlike interactions of internal constituents of quarks. Figure 1a shows, for illustration, the expected jet spectrum resulting from a 4-Fermi interaction characterized by a scale parameter Λ_C = 1400 GeV, the CDF limit from previous data [7].

Because of the steepness of the E_t distributions, modest uncertainty in knowledge of the absolute jet energy scale can have a significant effect (a factor of 5-6 larger than the scale variation itself) on overall knowledge of the spectra. To understand this calibration, techniques have been developed using collider data. CDF uses a combination of testbeam calorimeter calibrations (above 10 GeV) and information from charged particle momentum measurements in the CDF Central Tracking Chamber (CTC) as input to a detailed detector simulation tuned to reproduce the fragmentation properties of jets, and the effects of the CDF detector. D0 utilizes the expected E_t balance of events containing an energetic photon and a jet to normalize the jet energy scale to the well-measured electromagnetic energy scale. The systematic uncertainty obtained is about 4% for CDF and 10% for D0. With this knowledge, CDF performs a deconvolution of the effects of detector energy resolution to obtain a corrected jet spectrum. D0 convolves the theoretical curve with the resolution to form a direct comparison with observed data.

The current systematic uncertainty on the D0 measurement resulting from energy scale variation is shown in figure 1b as solid lines. CDF quotes a systematic error on the cross-section from all sources of approximately 20%.

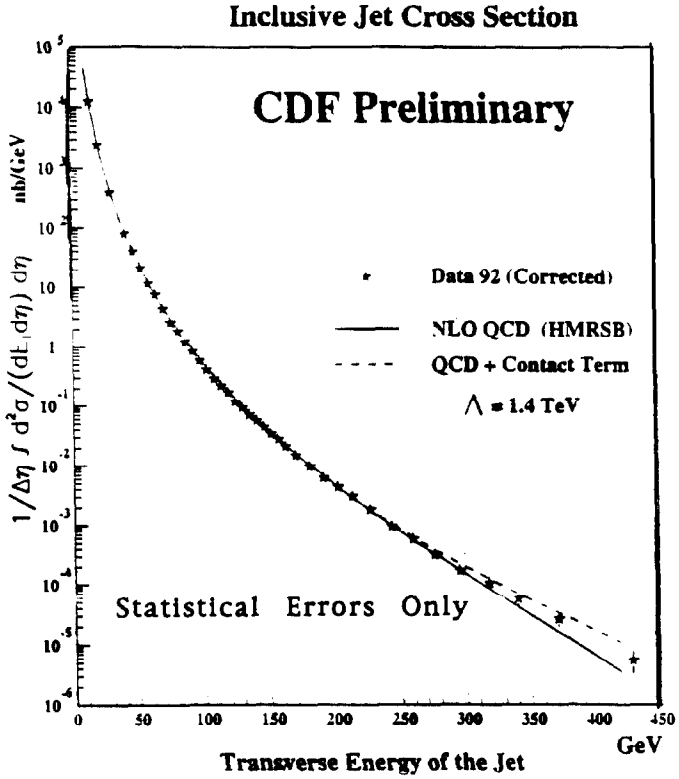

Figure 1a: Cross-section for inclusive jet production in $0.1 < |\eta| < 0.7$ from 14.3 pb^{-1} at CDF, compared to NLO predictions.

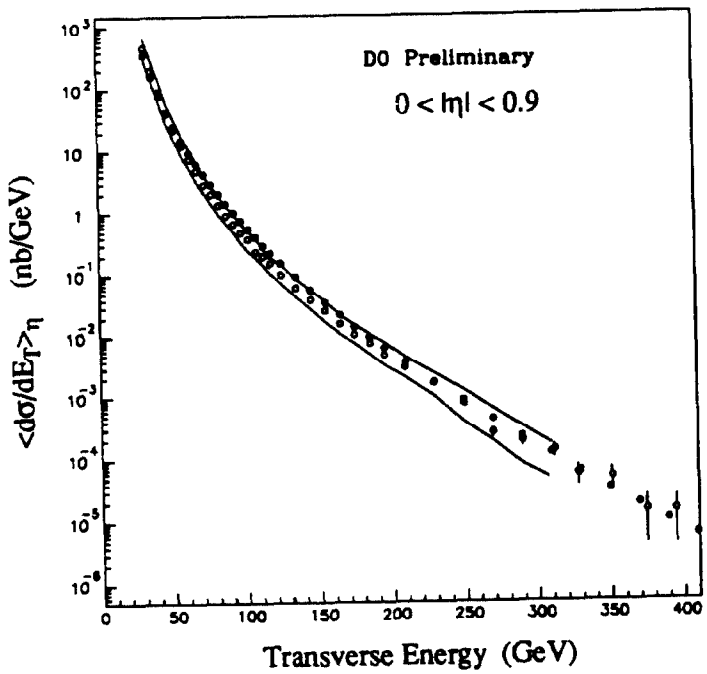

Figure 1b: D0 inclusive jet cross-section from 4 pb^{-1}. Open circles are data, closed circles NLO QCD prediction with HMRSB0 structure function at a scale $\mu = E_T / 2$. Solid lines show the uncertainty from energy scale.

Figures 2 and 3 illustrate the rapidity dependence of inclusive jet spectra, as measured by the two experiments. D0 uses its uniform calorimetry to measure the inclusive jet spectrum in the forward region of $2 < |\eta| < 3$. CDF utilizes the good resolution of the central calorimeter to fix the E_t of a dijet system (using the most energetic jet), and then plots the spectra separated into bins of second most energetic jet pseudo-rapidity. Figure 3 shows the spectra plotted as a ratio with the denominator being the spectrum where both leading jets are central. The ratio has many systematic uncertainties cancelling in the numerator and denominator, leaving a residual systematic as small as 4% in some regions, largely due to effects of different spectrum shapes convoluted with the energy scale uncertainty. At the large angular separation and high E_t , the momentum fraction x exceeds 0.7 for one of the incoming partons.

The center-of-mass angular distribution of dijets provides information about the hard scattering that is complementary to that provided by the inclusive jet spectrum. Factorization of the dijet cross-section results, in lowest order, in two terms, one of which depends on the parton distribution function and the other on the center-of-mass scattering angle θ^*. The angular distribution is a test of the spin structure of the fundamental hard scattering interaction.

Figure 4a shows the CM angular distribution of dijets as measured by D0. An earlier measurement by CDF [9] is shown in figure 4b. The measurements are displayed as functions of the reduced center-of-mass angular variable χ, where χ is defined as $\chi = (1 + \cos\theta^*) / (1 - \cos\theta^*)$, and is expected to be flat for pure Rutherford scattering. Fiducial cuts are applied in $\eta_{boost} = 1/2 (\eta_1 + \eta_2)$ and in $\eta^* = 1/2 (\eta_1 - \eta_2)$, to insure a uniform acceptance and trigger efficiency as a function of χ. Here η_1 and η_2 are the pseudo-rapidities of the most energetic and second most energetic jets. These cuts, along with the trigger

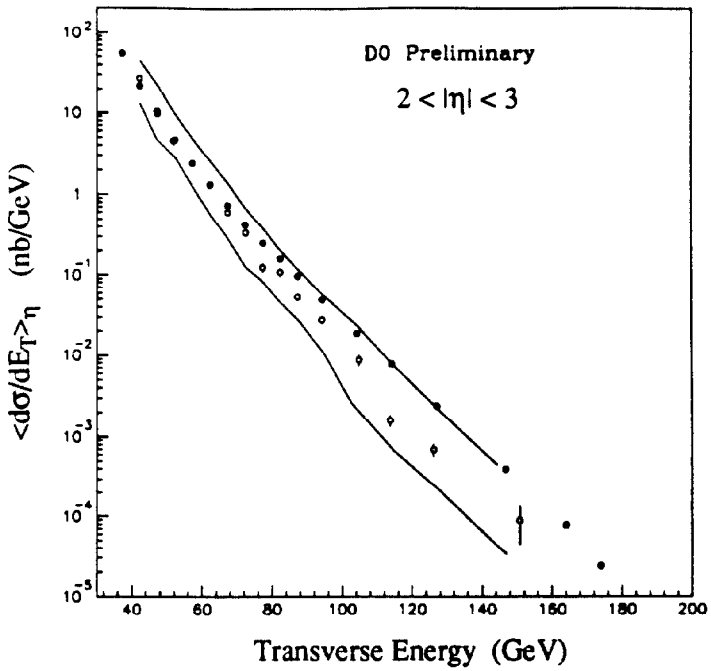

Figure 2: D0 inclusive jet cross-section in forward region. Open circles are data, closed circles NLO QCD prediction. Uncertainty as in figure 1b.

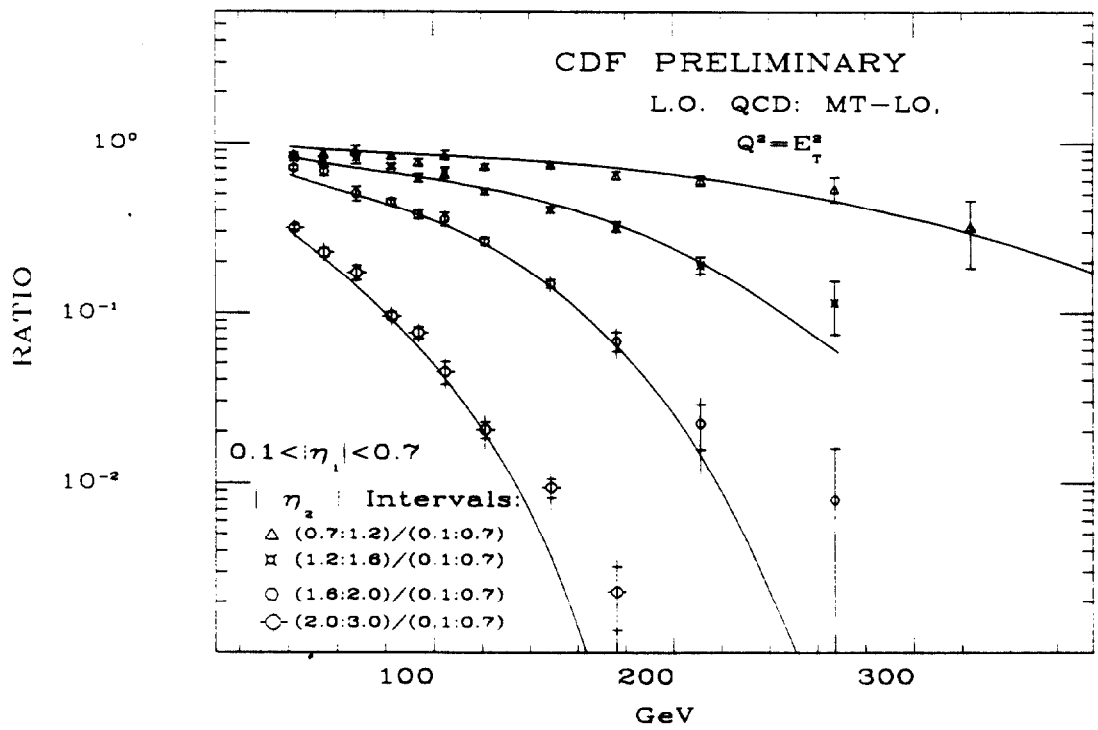

Figure 3: Ratio of CDF differential jet cross-section with one central jet to cross-section with both jets central, for varying second jet rapidity. Inner error bars statistical, outer statistical and systematic in quadrature.

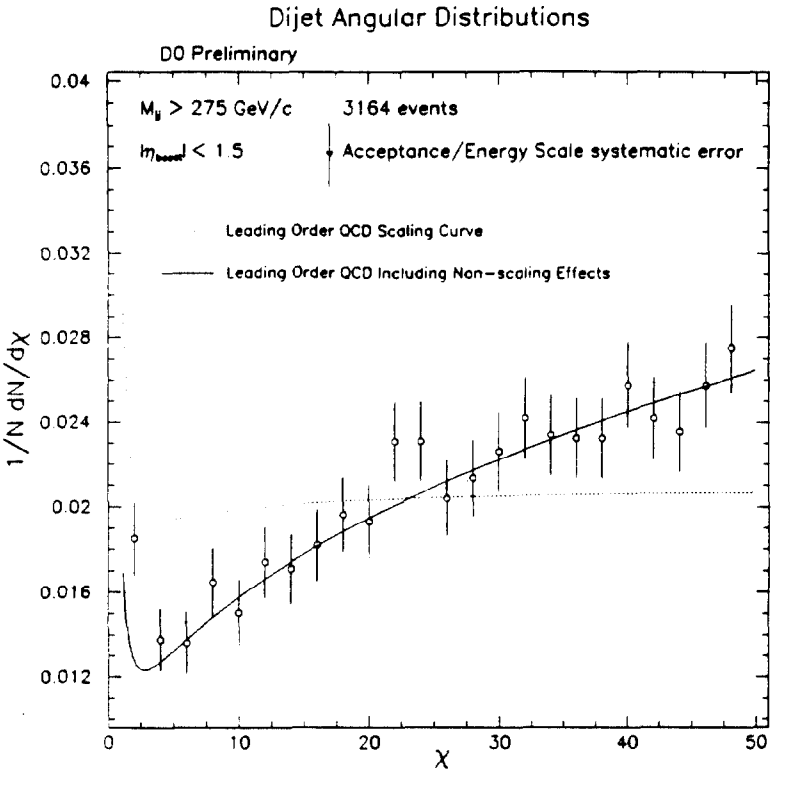

Figure 4a: D0 jet center-of-mass angular distribution as a function of reduced angular variable χ,

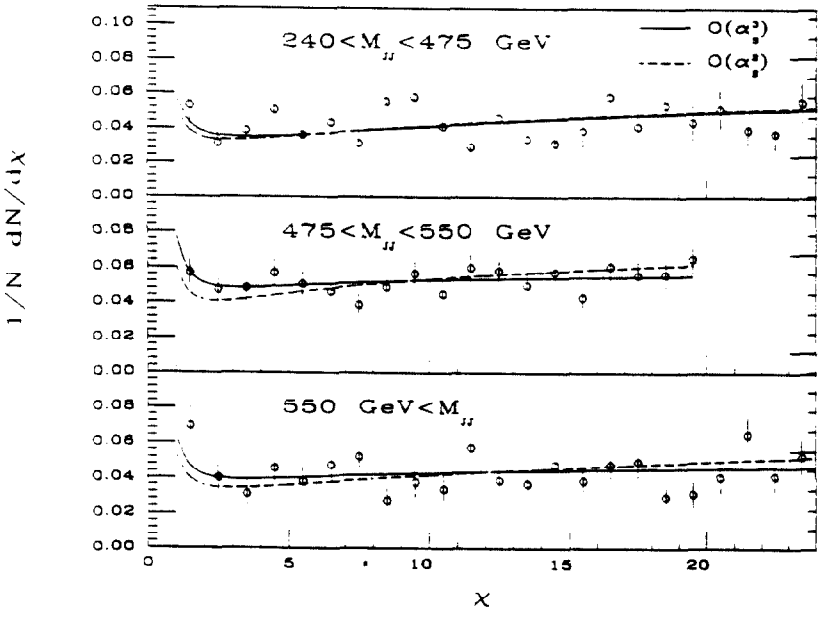

Figure 4b: CDF jet angular distribution from reference [9].

threshold in E_t , determine the maximimum available χ. CDF requires $|\eta_{boost}| < 0.75$ and achieves a maximum χ of 24, which corresponds to a maximum jet η of 2.3. The D0 distribution extends to χ of approximately 50 ($\eta < 3.0$). Both distributions show good agreement with the QCD predictions. For this distribution, the leading order and NLO predictions are similar.

Another way to study events containing jets is to trigger on the total deposited transverse energy in the detector. Figure 5a displays a LEGO plot of the CDF event with the highest total E_t observed in the 1992-93 running period. In this analysis the E_t is computed using only clusters of at least 10 GeV each. Defined in this way, the mean total E_t of the event is expected to contain less than a 1.5% contribution from additional interactions in the same beam crossing. Figure 5b shows the spectrum of CDF events containing more than 320 GeV E_t, compared to a prediction of the HERWIG shower Monte Carlo (after detector simulation).The Monte Carlo calculation has been normalized upwards by a factor of 1.5 to account for the observed cross-section of 387 pb. CDF has previously published a detailed analysis of the characteristics of events selected in a similar fashion from earlier data [10].

Direct Photon Production

QCD predicts the occurence of events containing an energetic direct photon and jets from hard scattering interactions. These photons are produced in the processes $qg \rightarrow \gamma q$ and $q\bar{q} \rightarrow \gamma g$. There is also a significant contribution (approx. 40% at $E_t(\gamma) = 20$ GeV) from the bremsstrahlung process $qg \rightarrow qg + \gamma$. Photons are identified in CDF and D0 as isolated electromagnetic calorimetric clusters with no associated charged track. CDF requires less than 2 GeV of additional E_t in a cone of $R = 0.7$ around the electromagnetic cluster; D0 requires that less than 15% of the cluster's E_t be deposited in a annular region between R=0.2

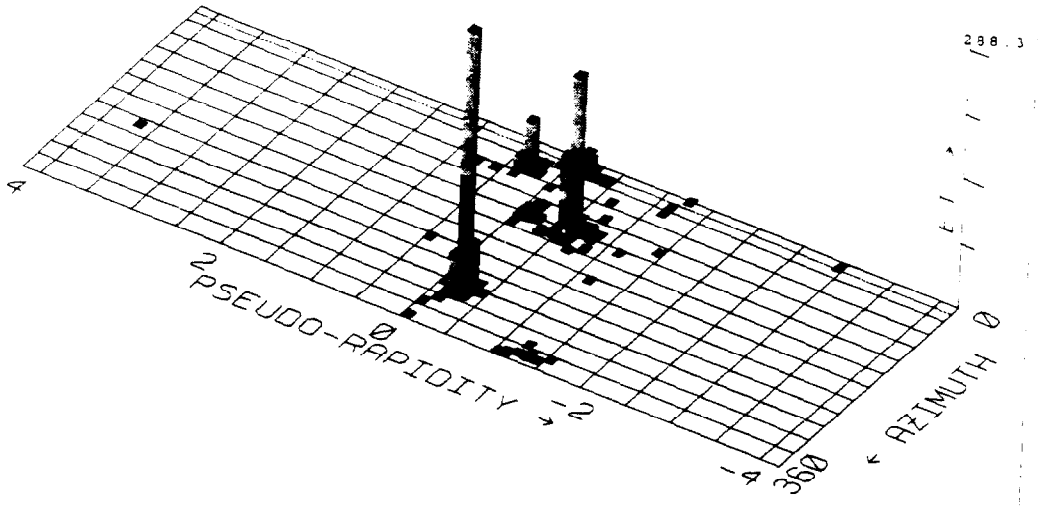

Figure 5a: CDF event with highest total transverse energy.

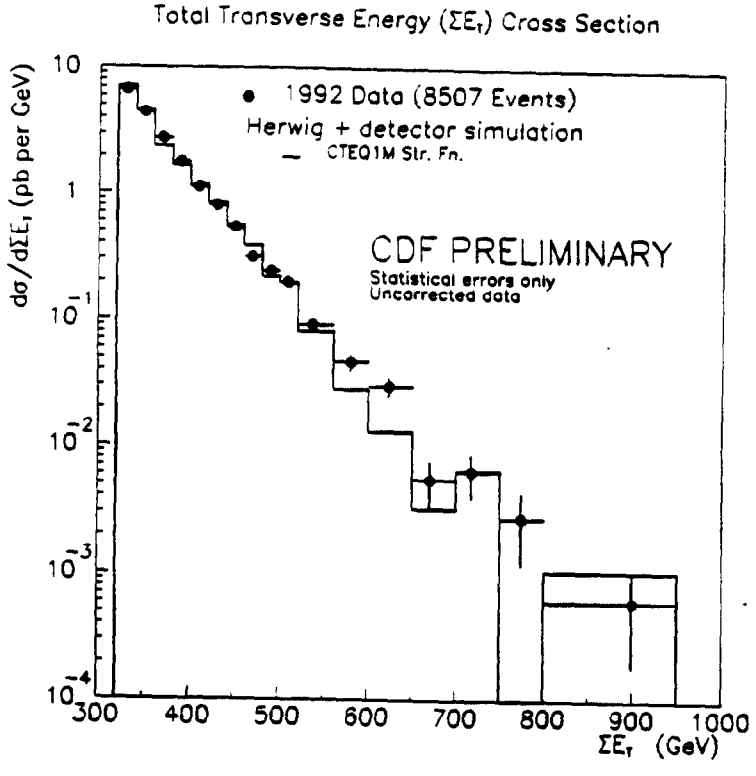

Figure 5b: CDF transverse energy distribution compared with predictions of the HERWIG Monte Carlo. Results are from 22 pb^{-1}.

and R=0.4. CDF further isolates good photon candidates by cutting on the statistical likelihood that a real photon would have a transverse shower profile similar to the observed cluster, as measured in CDF's Central Electromagnetic Strip (CES) detectors, which are embedded in the Central Electromagnetic Calorimeter (CEM) at a depth of approximately 6 radiation lengths.

The major background to direct photons comes from QCD dijet production, where one of the jets has fragmented into a single π^0 or other neutral meson. In order to measure photon cross-sections and kinematical distributions, statistical techniques are employed. CDF uses two background subtraction techniques [11]. In the E_t range below 18 GeV, shower CES profiles are compared with expected photon shapes, and a χ^2 is formed for the cluster. Using knowledge of the expected distribution of this χ^2 for photon and background events (which is obtained from a combination of testbeam measurements using electrons and Monte Carlo simulations), an efficiency for a cut of $\chi^2 < 4.0$ can be computed for both signal (ε_γ) and background (ε_{bkg}). Then the fraction of photons can be computed using the equation $F_\gamma = \frac{\varepsilon_{bkg} - \varepsilon}{\varepsilon_{bkg} - \varepsilon_\gamma}$ where ε is the observed efficiency for the data to have $\chi^2 < 4.0$. The systematic uncertainty in this subtraction grows rapidly with E_t, as clusters from decaying π^0's become more collimated, and above E_t = 18 GeV, a different technique is used. Multiwire proportional chambers, the Central Preradiator Chambers (CPR) can be used to measure the relative probability of conversions in the 1.09 radiation lengths of the CDF solenoid and associated cryostat. These probabilities can then be used in a way similar to the profile technique to statistically extract fractions of photons and background. This conversion technique is useful to large values of the photon E_t, since the conversion efficiencies are approximately independent of energy. D0 similarly separates background from signal using conversions inside the central D0 detector, detected by dE/dx in the central drift chamber.

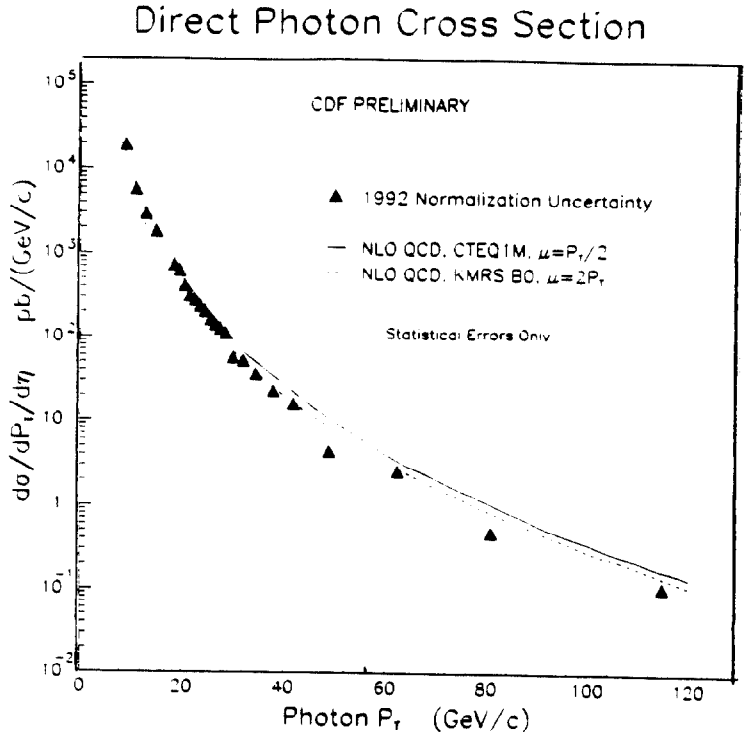

Figure 6a: CDF inclusive isolated photon cross-section.

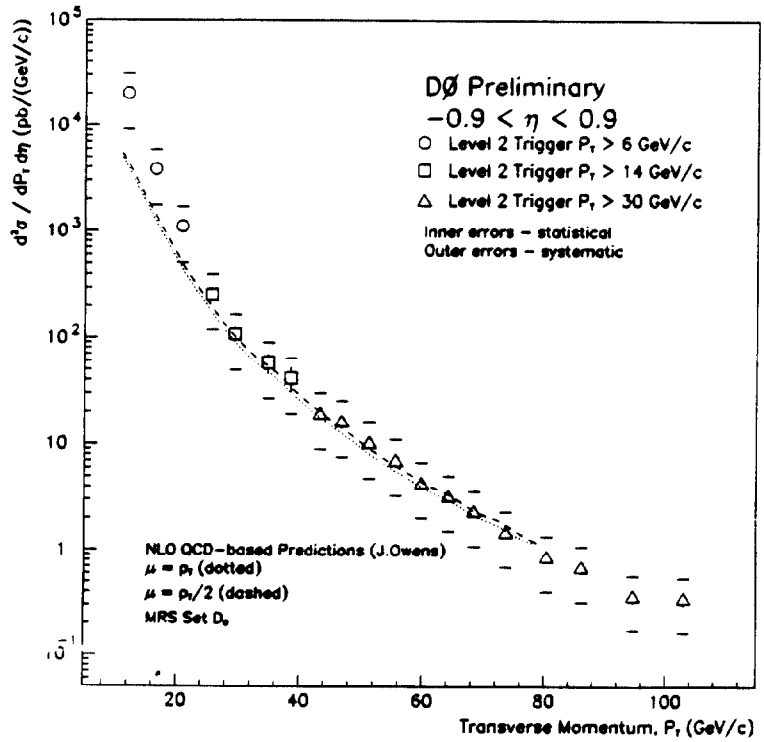

Figure 6b: Inclusive direct photon cross-section from D0.

Figures 6a and 6b show the direct photon spectrum as measured at CDF and D0. In both cases comparison is made with NLO QCD calculations [12,13]. The dominant systematic uncertainty is knowledge of the background subtraction, which ranges, for CDF, from 40% at low E_t, to approximately 17% at higher E_t. The CDF data show a systematic difference in shape from the NLO calculation. The D0 data also appear higher than the calculation at low E_t.

Using the background subtraction technique, one may obtain "signal" and "background" weights that allow event-by-event measurements of photon kinematic distributions. An example of this technique is shown in figure 7, where we plot the CDF result for the center-of-mass angular distribution for direct photons. Also shown is the converse distribution, the angular distribution for photon background. The background curve is seen to agree well with a leading-order QCD calculation for dijet production [14]. The NLO calculation for the photon angular distribution [13] lies somewhat below the data at high values of $\cos\theta^*$. All data and theory curves are normalized to have equal areas in the region below $\cos\theta^* < 0.3$.

QCD also predicts the existence of diphoton events from a combination of $q\bar{q}$ annihilation, double bremsstrahlung, and higher-order gluon fusion processes. Figure 8 shows a preliminary CDF measurement of the diphoton mass spectrum. The data is compared to a NLO calculation [15], and an estimate of the background. The background estimate is derived by estimating the probability that a jet fragments into a single electromagnetic cluster, using the signal and background fractions from single photon data and the relatively well-known jet and single photon cross-sections. The theory curve has been multiplied by a factor of 1.24 to normalize it to the data at 50 GeV. Using 18 pb^{-1} of data we find two diphoton events of mass above 350 GeV/c^2.

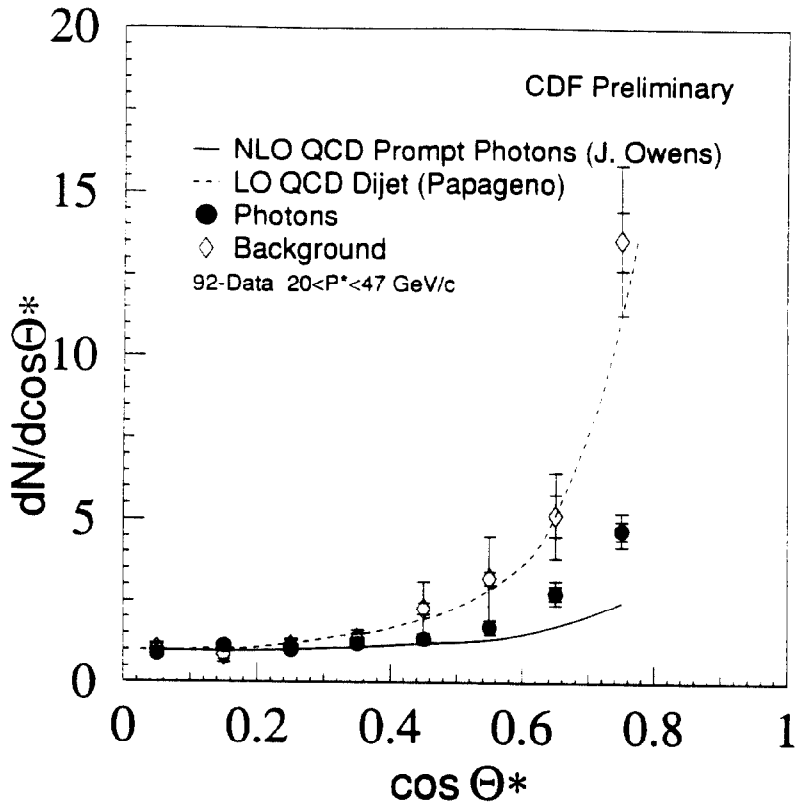

Figure 7: Distribution of cosθ* for direct photons and background. Inner error bars statistical, outer statistical and systematic in quadrature.

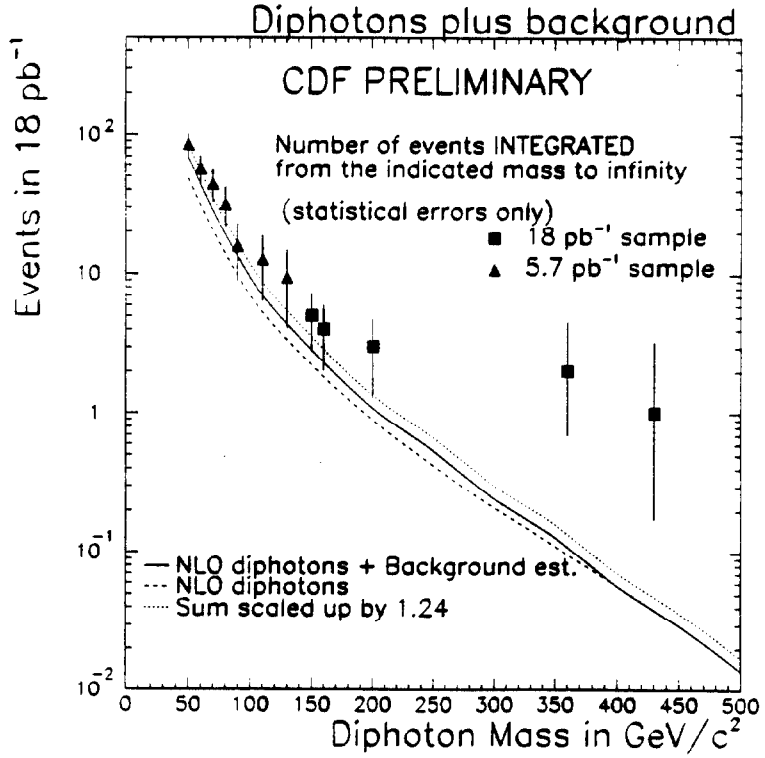

Figure 8: Invariant mass distribution for events with energetic diphotons. Theory normalized to data at 50 GeV/c^2.

W + Jets Production

W bosons are often produced in association with QCD jets. At 1.8 Tev, CDF has published, from earlier data, a measurement of the W production cross-section as a function of the multiplicity of jets above 15 GeV E_t in the events [16], compared to recent complete leading-order calculations [17]. Currently, a NLO calculation of the W + 0 jet and W + 1 jet production cross-sections has become available [4]. D0 has used 14.3 pb^{-1} of recent data to make a comparison with this prediction.

W bosons are identified in D0 as energetic isolated electrons with significant missing E_t , indicating a neutrino. Electrons are required to have $P_t > 25$ GeV; the missing E_t must also be greater than 25 GeV. Transverse shower shape cuts are applied to enhance the signal. The overall efficiency for W selection is approximately 31%. Figure 9a shows the D0 W + jet multiplicity distribution for various values of the jet threshold. Errors shown are statistical, and backgrounds have not been subtracted. The curves shown are illustrative exponential fits.

In figure 9b, we see that the ratio of the number of events with a W boson and an energetic jet to those with only a W depends on the strong coupling constant α_s. The measured distribution is plotted as a function of the minimum jet E_t , and is compared to a NLO calcuation using the DYRAD program [4] with MRSD0 structure functions and a renormalization scale $\mu = M_W$. Since the distribution is a ratio of falling spectra, the systematic error from the jet energy scale uncertainty is 22-25%, and is displayed with the points. Electroweak backgrounds arising from processes such as $Z^0 \rightarrow e^+ e^-$ (with one leg misidentified as a jet), or $Z^0 \rightarrow \tau^+ \tau^-$ (with one t decaying to hadrons) total about 1% and have been subtracted. There remains a significant

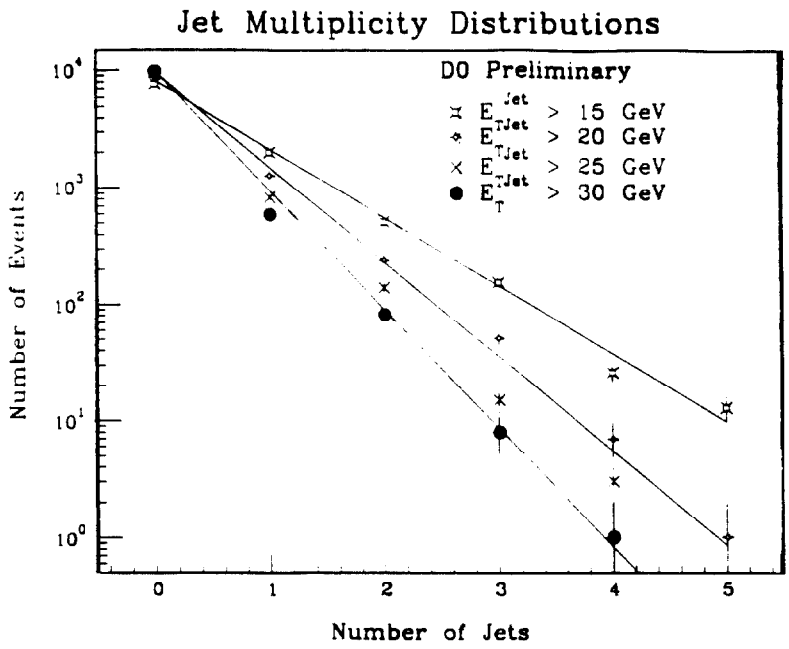

Figure 9a: D0 jet multiplicity distribution in events containing a W, for various values of the jet transverse energy threshold.

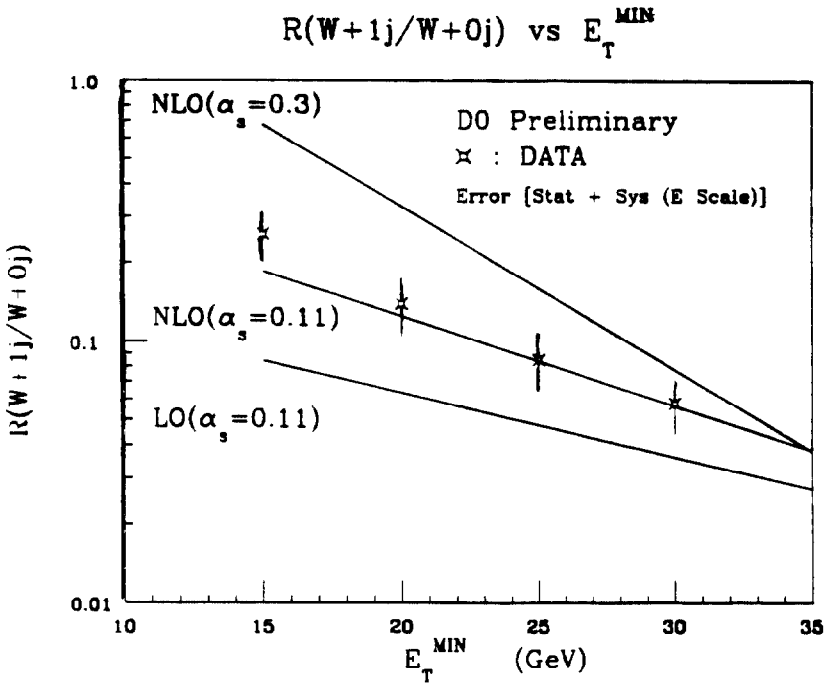

Figure 9b: Ratio of rate for events containing a W and one jet to events with a W and no energetic jet, as a function of jet threshold. Results are compared to predictions of DYRAD Monte Carlo.

background of two-jet events in which one jet mimics an electron, which is expected to be on the order of 20%.

Study of Parton Distribution Functions

The high center-of-mass energy of the Tevatron collider makes it possible to obtain events with energetic jets and photons at low values of the momentum fraction x. Special kinematic configurations are selected to take advantage of the defining relations for x in terms of transverse energy and rapidity in a two-body system:

$$x_{a(b)} = \frac{E_t}{\sqrt{s}} \left(e^{(-)\eta_1} + e^{(-)\eta_2} \right).$$

Here x_a and x_b are the momentum fractions of the incoming partons, η_1 and η_2 are the pseudo-rapidities of the outgoing partons, and E_t is their common transverse energy in this two-body approximation. Events with both 2 energetic jets and with a jet/photon combination have been studied by CDF. Since interaction rates in general depend on the parton distribution functions at the x-values of the incoming partons, these classes of events will provide useful constraints on these functions.

Figure 10 shows the ratio of observed events with two energetic same-side jets to those with two jets on opposite sides in η, as a function of the pseudo-rapidity of the leading jet η_1. The events are required to have a second jet above 5 GeV in observed E_t, and the azimuthal separation $\Delta\phi$ is required to lie in the range $\pi - 0.7 < \Delta\phi < \pi + 0.7$. The ratio is compared to predictions of leading order QCD for a variety of structure functions. There is some evidence for more singular gluon distributions. Statistical errors are plotted in the figure. The measurement is limited by statistics with 9.4 pb^{-1} of luminosity. Although systematic errors on the measured ratio will be small, there is an ambiguity in

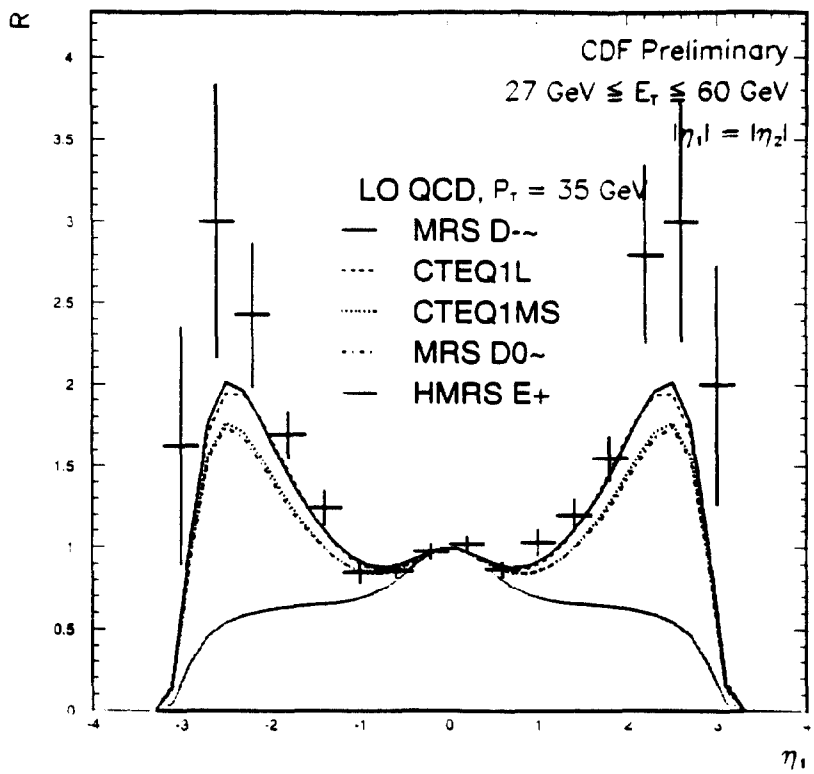

Figure 10: CDF measured ratio of same-side/opposite-side jet pairs as a function of pseudo-rapidity in the range 27 GeV < E_t < 60 GeV.

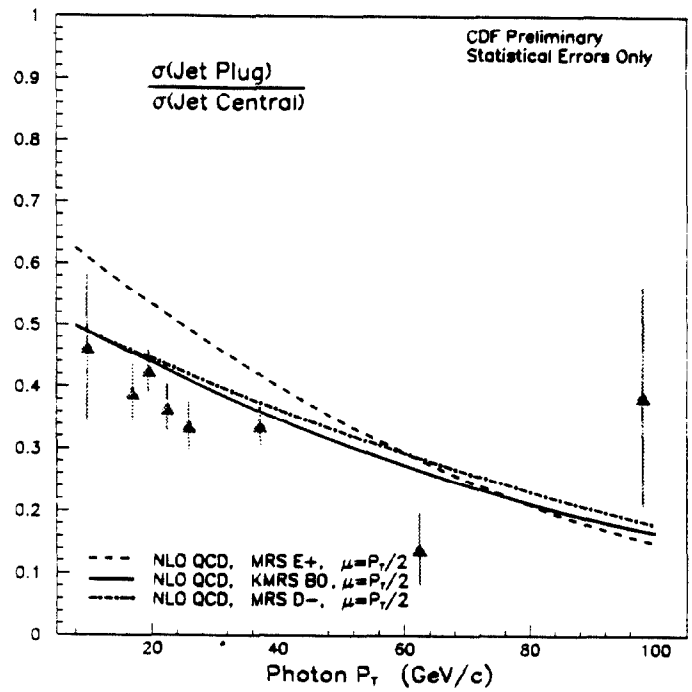

Figure 11: Ratio of CDF photon + jet cross-sections, for the case with a jet in the endplug region compared to the cross-section with a central jet.

comparison with theoretical predictions, since the mean value of E_t will vary as a function of η_1, due to convolution of the dijet differential cross-section (whose steepness varies with η) with the detector energy resolution.

Figure 11 shows another ratio measurement of CDF, using events with one jet and a photon. Here the numerator is formed from events with a jet in the CDF endplug region, $1.4 < |\eta_{jet}| < 2.2$. At a photon P_t of 7 GeV/c, this configuration probes x down to 0.004. In the denominator the jet is restricted to the central region, $|\eta_{jet}| < 0.9$. In both cases the photon is central ($|\eta_\gamma| < 0.9$). Theoretical predictions [13] for 3 sets of parton distribution functions are shown. The data lie somewhat below the predictions, and the older extreme case HMRSE+ is disfavored.

Search for Events with Rapidity Gaps

In QCD hard scattering events the space between jets is typically filled with soft fragmentation products, which may be described as coming from a color string created in the original exchange. Another class of predicted events containing jets [18] may result from the exchange of a colorless object such as a Pomeron (modeled as a colorless combination of gluons). These events should have fewer underlying fragmentation products and will exhibit a region between jets depleted in particles, a "rapidity gap". Figure 12 schematically indicates the structure of such an event. These events may provide a useful clean region to observe decay products of heavy objects produced at higher energies.

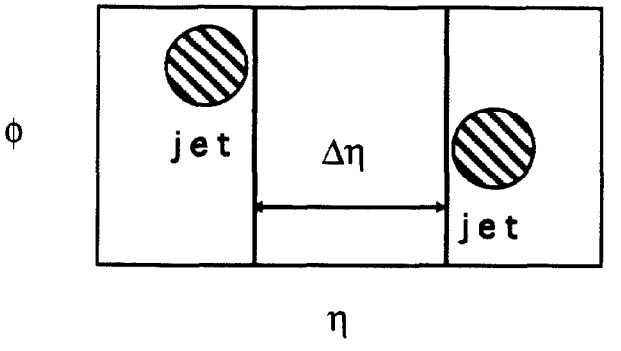

Figure 12: Structure of an event containing a rapidity gap and jets. No particles are found in the central region.

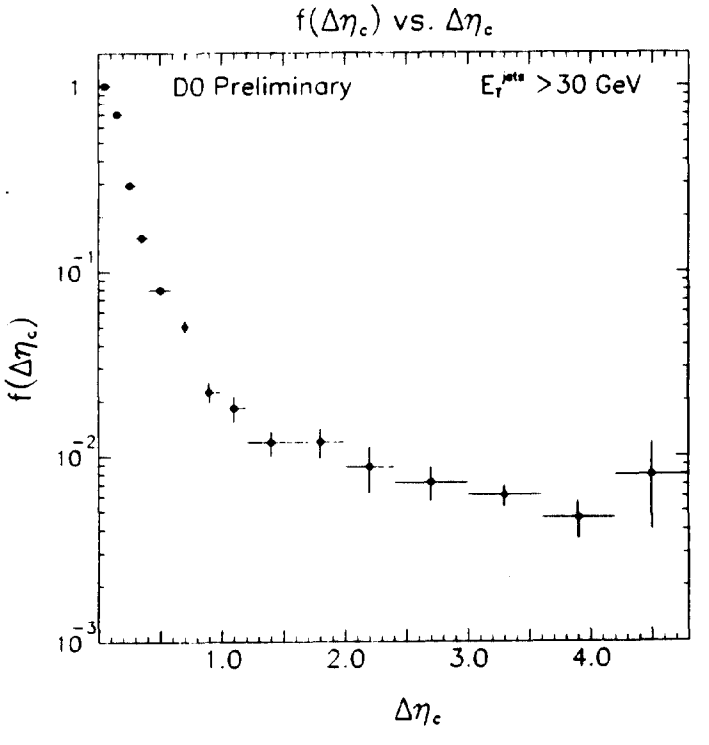

Figure 13: D0 observed fraction of events containing a rapidity gap as a function of gap width $\Delta\eta$. Statistical errors only.

The fraction of observed events with a rapidity gap $\Delta\eta$ (defined as $\Delta\eta = |\eta_1 - \eta_2| - 1.4$, to correct for the finite radius of R = 0.7 jet cones), may be expressed as

$$f(\Delta\eta) = \frac{\sigma_{gap}(\Delta\eta)\, S}{\sigma(\Delta\eta)},$$

where $\sigma_{gap}(\Delta\eta)$ is the cross-section for events with $\Delta\eta$ between the two leading jets and no detected activity in the gap, $\sigma(\Delta\eta)$ is the total cross-section for dijet events with such a gap, and S is the probability that the gap is not masked by a fluctuation of the spectator underlying event. Similarly, underlying events and jet fragmentation can fluctuate in such a way as to create a gap in an event produced by exchange of quarks and/or gluons. These "fake gaps" constitute a background to $f(\Delta\eta)$; their distribution is expected to be approximately exponential in $\Delta\eta$. In contrast, the signal of gaps from colorless exchange is expected to be flatter as a function of $\Delta\eta$.

Figure 13 shows preliminary D0 results for $f(\Delta\eta)$. The event selection requires 2 jets above 30 GeV E_t. An event is classified as a gap event if no electromagnetic calorimeter tower in the gap has appreciable E_t (with a threshold of 200 MeV). The fraction declines as expected, and shows a flattening above $\Delta\eta = 2.0$. There are systematic effects that can both increase $f(\Delta\eta)$ (such as noisy towers in the gap, which reject events that should pass) , and decrease it (such as the efficiency for a single particle to deposit adequate energy to pass the tower threshold). D0 believes that it is unlikely that the true baseline of $f(\Delta\eta)$ is greater than 1%.

B Meson Differential Cross-Section

Heavy quark production in hadron collisions provides a stringent test of perturbative QCD as applied to exclusive channels. A very large number of b-quarks are produced at the Tevatron due to the high center-of-mass energy. CDF has published a number of measurements of the b-quark production cross-section at $\sqrt{s}$ = 1800 GeV. (For a recent overview, see reference [19]). Some of these measurements require assumptions, such as the shape of the P_t spectrum of the produced b-quarks, or the mechanism of production of J/Ψ final states. Fully reconstructed final states require only knowledge of the fragmentation of b-quarks to B mesons as theoretical input to extract the b-quark cross-section.

Exclusive B meson final states are identified by their decays into modes including a J/Ψ particle in the modes $B^+ \rightarrow J/\Psi + K^+$ and $B^0 \rightarrow J/\Psi + K^{*0}$ (and their charge conjugates), with the J/Ψ decaying to $\mu^+\mu^-$. This decay of the J/Ψ is identified at the trigger level, beginning with the requirement of two muons found in the central muon chambers. At least one of the tracks must match a track found in the CTC by a fast hardware track processer whose efficiency is 50% at 2.7 GeV/c, rising to 90% at 3.4 GeV/c. We later require that each muon have $P_t > 1.8$ GeV/c, and that at least one muon have $P_t > 2.8$ GeV/c , and that the muons have opposite charge and originate from a common vertex.

Figure 14 shows the reconstructed mass of the dimuon pair (constrained to the J/Ψ mass), and K^+ candidates found in the CTC. The dimuons are required to fall within 3σ of the J/Ψ mass before inclusion, where σ is determined from a Gaussian fit to the J/Ψ mass peak observed in the data. K^+ candidates must have

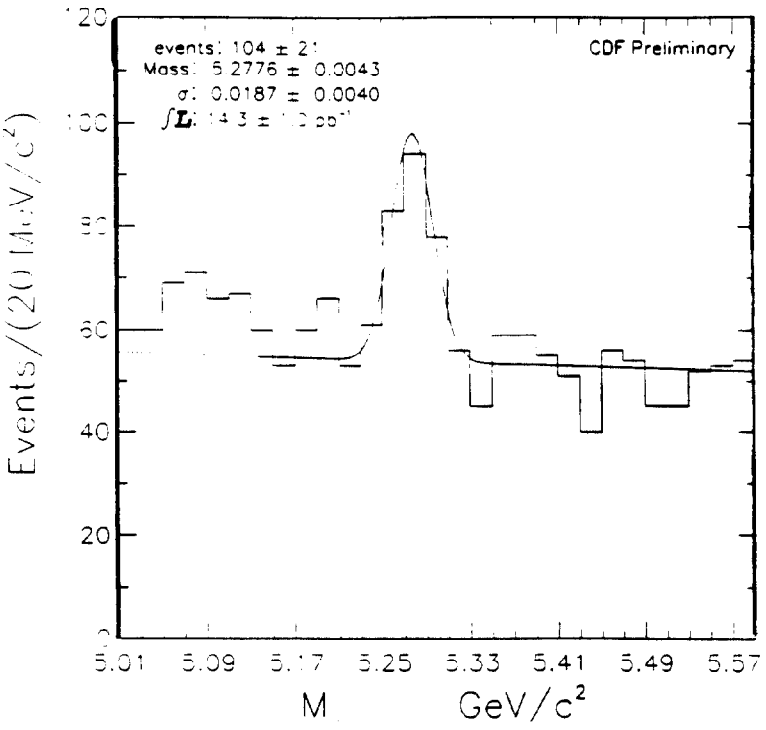

Figure 14: CDF invariant mass distribution for charged B candidates.

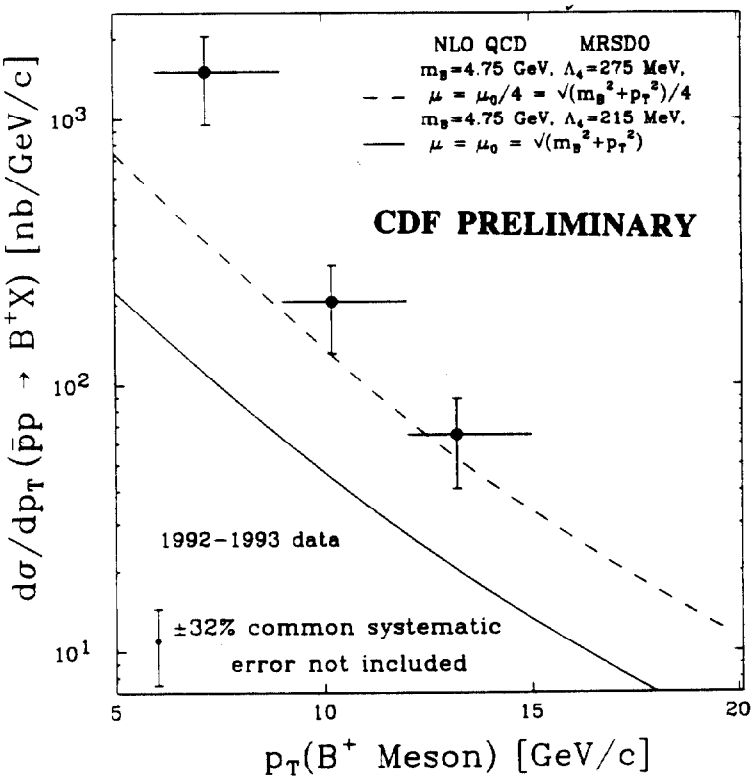

Figure 15: CDF differential cross-section for production of B mesons.

$P_t > 2.0$ GeV. All tracks have been refit, constrained to a common vertex. At the mass of the B^+ a signal is clearly apparent. A Gaussian with a linear background has been fit to the data in the region marked with the solid line. Similar analysis for the mode $J/\Psi + K^{*o}$ yields a signal of 26 ± 8 reconstructed B^o events.

In figure 15, the reconstructed B^+ mesons have been used to form the differential cross-section for the exclusive channel $p\bar{p} \longrightarrow B^+ X$. A common systematic of 32% (dominated by the branching ratio for $B^+ \longrightarrow J/\Psi K^+$) has been separately displayed. The errors shown are a quadrature combination of statistical and remaining systematic errors. All points are corrected for acceptance and efficiency. Also shown is a comparison with NLO QCD predictions [20]. It suggests that the theoretical cross-section differs somewhat in shape and normalization from the CDF measurement.

Conclusions

Tevatron collider experiments have already provided, and continue to provide, many important tests of perturbative QCD. In the most recent data, CDF and D0 have investigated inclusive jet and photon processes, and are now also studying processes exclusive in either kinematic variables or specific final state particles. As the theoretical understanding of QCD has advanced, experimentalists are challenged to focus on sensitivity. This productive dialog will continue as more data makes more and more of the full range of QCD production processes accessible.

References

[1] T. Akesson et al.,Phys. Lett. **118B**, 185 (1982).
M. Banner et al.,Phys. Lett. **118B**, 203 (1982).
G. Arnison et al.,Phys. Lett. **123B**, 115 (1983).

[2] F. Aversa et al., Phys. Lett. **B210**, 225 (1988).
S. Ellis, Z. Kunszt, and D. Soper, Phys. Rev. Lett. **62**, 2188 (1989).
S. Ellis, Z. Kunszt, and D. Soper, Phys. Rev. Lett. **64**, 2121 (1990).

[3] S. D. Ellis, Z. Kunszt, and D. E. Soper, Phys. Rev. Lett. **69**, 1496 (1992).

[4] W.T. Giele, E.W.N. Glover, and D.A. Kosower, FERMILAB-PUB-92/230T, 1992
H. Baer and M. H. Reno, FSU-HEP-901030 (1990).

[5] G. Marchesini and B. R. Webber, Nucl. Phys. **B310**, 461 (1988).

[6] T. Sjostrand, Comp. Phys. Comm. **39**, 347 (1986).
T. Sjostrand and M. Bengtsson, Comp. Phys. Comm. **43**,

[7] F. Abe et al., Phys. Rev. Lett. 68, **1104**, (1992).

[8] F. Abe et al., Phys. Rev. **D48**, 998 (1993).

[9] F. Abe et al., Phys. Rev. Lett. **69**, 2896 (1992).
367 (1987).

[10] F. Abe et al., Phys. Rev. **D45**, 3921 (1992).

[11] F. Abe et al., Phys. Rev. **D48**, 2998 (1993).

[12] J. Ohnemus, H. Baer and J. F. Owens, Phys. Rev. **D42**, 1 (1990).

[13] H. Baer, J. Ohnemus and J.F. Owens, Phys. Lett. **234B**, 127 (1990).

[14] I. Hinchcliffe, PAPAGENO Event Generator, private communication.

[15] B. Bailey, J. F. Owens and J. Ohnemus, Phys. Rev. **D46**, 2018 (1992).

[16] F. Abe et al., Phys. Rev. Lett. **70**, 4042 (1993).

[17] F. A. Berends, W. T. Giele, H. Kuijf and B. Tausk, Nucl. Phys. **B357**, 32 (1991).

[18] Y. Dokshitzer, V. Khoze, and S. Troyan, *Proceedings of the 6th International Conference on Physics in Collision (1986)*, ed. M. Derrick (World Scientific, Singapore, 1987).
J. D. Bjorken, Phys. Rev. **D47**, 101 (1992).

[19] B. T. Huffman, FERMILAB-CONF-93/274-E

[20] M. Mangano et al., Nucl. Phys. B373, 295 (1992).
M. Mangano, IFUP-TH 2/93 (INFN Pisa), 1993.